JGR Oceans

RESEARCH ARTICLE
10.1029/2020JC016600

Winter Air-Sea CO_2 Fluxes Constructed From Summer Observations of the Polar Southern Ocean Suggest Weak Outgassing

Neill Mackay[1] **and Andrew Watson**[1]

[1]Laver Building, University of Exeter, Exeter, UK

Key Points:

- Wintertime observations of surface partial pressure of CO_2 (pCO_2) south of the Polar Front in the Southern Ocean are reconstructed using subsurface winter water identified in summertime observations, greatly improving wintertime spatiotemporal coverage
- We combine our reconstructed wintertime observations with other available observations of surface pCO_2 and use a multiple linear regression to produce a gap-filled map from which we estimate air-sea CO_2 fluxes for 2004–2017
- The addition of the reconstructed observations increases winter outgassing south of the Polar Front when compared with an estimate based on shipboard observations of surface pCO_2

Correspondence to:
N. Mackay,
n.mackay@exeter.ac.uk

Citation:
Mackay, N., & Watson, A. (2021). Winter air-sea CO_2 fluxes constructed from summer observations of the polar Southern Ocean suggest weak outgassing. *Journal of Geophysical Research: Oceans*, *126*, e2020JC016600. https://doi.org/10.1029/2020JC016600

Received 10 JUL 2020
Accepted 6 APR 2021

Abstract The Southern Ocean plays an important role in the global oceanic uptake of CO_2. Estimates of the air-sea CO_2 flux are made using the partial pressure of CO_2 at the sea surface (pCO_2^{surf}), but winter observations of the region historically have been sparse, with almost no coverage in the Pacific or Indian ocean sectors south of the Polar front in the period 2004–2017. Here, we use summertime observations of relevant properties in this region to identify subsurface waters that were last in contact with the atmosphere in the preceding winter, and then reconstruct "pseudo observations" of the wintertime pCO_2^{surf}. These greatly improve wintertime coverage south of the Polar Front in all sectors, improving the robustness of flux estimates there. We add the pseudo observations to other available observations of pCO_2^{surf} and use a multiple linear regression to produce a gap-filled time-evolving estimate of pCO_2^{surf} from which we calculate the air-sea flux. The inclusion of the pseudo observations increases outgassing at the beginning of the period, but the effect reduces with time. We estimate a 2004–2017 long-term mean flux of -0.02 ± 0.02 Pg C yr^{-1} for the Southern Ocean south of the Polar Front, similar to comparable studies based on shipboard pCO_2^{surf} data. However, we diverge somewhat from an estimate which utilized autonomous float data for recent years: we find a small sink in 2017 of -0.08 ± 0.03 Pg C yr^{-1} where the float-based estimate suggested a small source.

Plain Language Summary The Southern Ocean is an important region where carbon dioxide (CO_2) gets absorbed into the ocean, however, the observations that allow us to calculate the flux are lacking. Estimates of the atmosphere-ocean flux of CO_2 rely on observations of surface CO_2 concentrations collected on board ships, which are especially sparse in the winter and in the most southerly parts of the Southern Ocean. In this study, we have used observations from below the surface taken in summertime to reconstruct estimates of the wintertime surface CO_2 concentrations, which we then use to estimate the flux. Focusing on the period 2004–2017, we estimate CO_2 fluxes between the ocean and atmosphere in the most southerly parts of the Southern Ocean that are broadly in line with other studies over the long-term mean, but which differ somewhat for recent years.

1. Introduction

The ocean is an important sink for anthropogenic CO_2, having absorbed 25% of that emitted between 1750 and 2018, and it, therefore, has a mitigating impact on climate change (Friedlingstein et al., 2019). The Southern Ocean is the largest oceanic sink of anthropogenic CO_2, representing around 40% of the contemporary sink (Devries, 2014), and accounting for 43% of the global oceanic uptake from 1861 to 2005 according to models (Frölicher et al., 2015). This substantial uptake of anthropogenic CO_2 is partially balanced by substantial outgassing of natural CO_2 supplied by the dense waters rich in dissolved inorganic carbon (DIC) which upwell to the surface in the Southern Ocean (Gruber et al., 2009).

The variability in the air-sea flux of CO_2 in the Southern Ocean is dominated by the seasonal cycle of ΔpCO_2, the difference between the partial pressure of CO_2 in the atmosphere and the surface ocean (Mongwe, Chang, & Monteiro, 2016). This in turn is driven by the seasonal cycle of the sea surface pCO_2, which depends on sea surface temperature (the thermal component) and biogeochemistry, including DIC, alkalinity, and salinity (the non-thermal component). Observational estimates find that pCO_2^{surf} in the high-latitude Southern Ocean has a peak in August (Austral winter) and a minimum in January (Austral summer), with the changes dominated by the non-thermal component (Landschützer, Gruber, Bakker, Stemmler, &

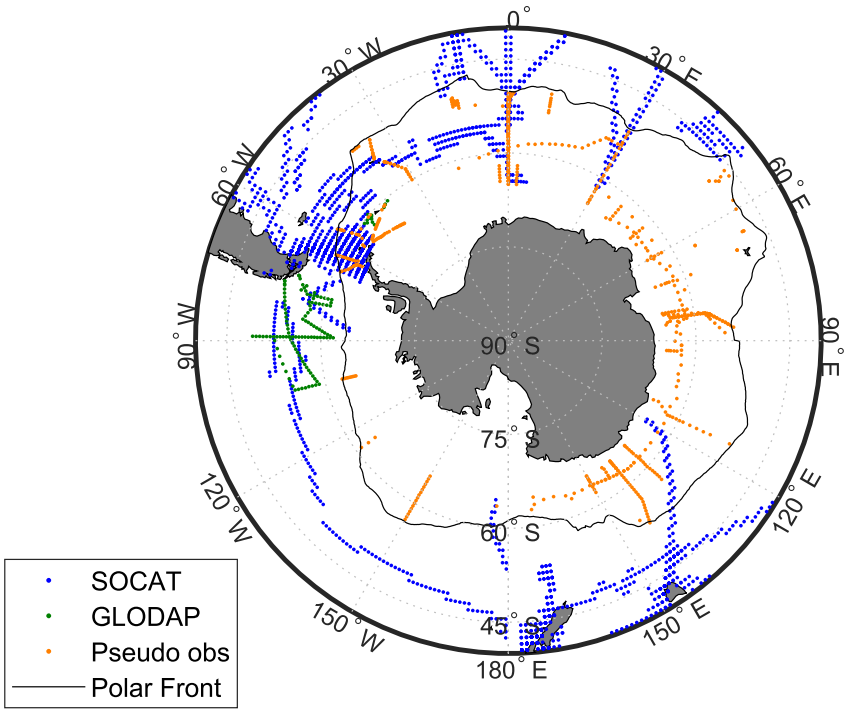

Figure 1. Wintertime (June to September) coverage of pCO_2^{surf} observations south of 40°S from 2004 to 2017. The blue dots are points in the 1° × 1° lat/lon gridded version of SOCAT (Bakker et al., 2016). The green dots are stations in GLODAP (Olsen et al., 2019) where we have calculated pCO_2^{surf} from other observations of the carbonate system, and the orange dots are the locations of our pseudo observations of pCO_2^{surf} (Section 2). The gray line gives the mean location of the Polar Front calculated from Freeman and Lovenduski (2016).

Six, 2018; Takahashi, Sutherland, Sweeney, et al., 2002). Observations of pCO_2^{surf} or its driving variables from both seasons are therefore required in order to constrain the air-sea flux.

Estimates of the air-sea flux of CO_2 from observations have traditionally used the sea surface partial pressure of CO_2 from ships and moorings. Existing observations of pCO_2^{surf} have been compiled in the Surface Ocean CO_2 Atlas (SOCAT, Bakker et al., 2016), and they are sparse in the Southern Ocean, particularly so in the wintertime and south of the Polar Front (see Figure 1). The available observations are used to generate time-evolving synoptic maps of pCO_2^{surf} by one of a number of gap-filling techniques (e.g., Gregor & Gruber, 2021; Landschützer, Gruber, Bakker, & Schuster, 2014; Rödenbeck, Keeling, et al., 2013; Takahashi, Sutherland, Wanninkhof, et al., 2009). The maps are then used in conjunction with atmospheric CO_2 data and a gas transfer parameterization to obtain the air-sea flux (see Section 4).

The sparsity of observations has meant that different observationally based estimates of the atmosphere-ocean CO_2 flux have their largest levels of disagreement in the Southern Ocean (Gregor et al., 2018; Rödenbeck, Bakker, et al., 2015). Despite this, an attempt by Gregor et al. (2017) to ascertain the effect of undersampling using model output found only a weak bias in ΔpCO_2. However the applicability of this result to the real ocean depends on the representation of the Southern Ocean in models, which has been shown to be poor (Lenton et al., 2013; Mongwe, Chang, & Monteiro, 2016). Mongwe, Vichi, and Monteiro (2018) found that CMIP5 Earth system models show excessive ingassing south of 65°S compared to observations, and that models mostly disagree with one another and with the observations on the seasonal cycle of the CO_2 flux. It has therefore been suggested that more observations are needed to reduce uncertainties in the Southern Ocean carbon sink and its variability, in particular south of the Polar Front (Fay et al., 2014; Mongwe, Vichi, & Monteiro, 2018).

In an attempt to address the sparsity of observations in the Southern Ocean, autonomous profiling floats began to be deployed in 2014 as part of the Southern Ocean Carbon and Climate Observations and Modeling

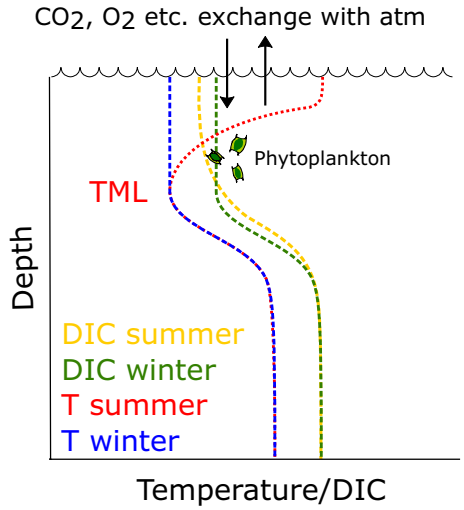

Figure 2. A representation of the temperature minimum layer (TML). The blue and red dashed lines show typical wintertime and summertime profiles of temperature with depth found south of the Polar Front in the Southern Ocean. The green and yellow dashed lines show typical wintertime and summertime profiles of dissolved inorganic carbon. Gases are exchanged with the atmosphere at the surface, and phytoplankton in the surface layer modify the concentrations of oxygen and DIC.

(SOCCOM) project (Johnson et al., 2017). The floats have pH sensors from which estimates of pCO_2^{surf} can be made, thereby substantially improving the spatiotemporal coverage of the Southern Ocean, especially in winter when the shipboard observations are most sparse. Using the SOCCOM float data, Gray et al. (2018) found stronger winter outgassing compared with previous estimates from shipboard pCO_2^{surf}, particularly between the Polar Front and the seasonal ice zone. Bushinsky, Landschützer, et al. (2019) (hereafter B2019) then combined the shipboard SOCAT data with SOCCOM float data, and used the pCO_2 mapping methods of Landschützer, Gruber, Bakker, Schuster, et al. (2013) and Rödenbeck, Keeling, et al. (2013) (hereafter R2013) to estimate the flux. They found weaker outgassing than Gray et al. (2018), but still a significant reduction in the overall sink compared with estimates using only SOCAT data. They also obtained different results depending on whether they used a combination of SOCAT and SOCCOM data or SOCCOM data only, raising the question of whether a lack of agreement in the two data sets was due to different sampling or a possible bias. They tested the effect of a possible bias of 4 μatm in the float-derived pCO_2 by subtracting a uniform value before carrying out the pCO_2 mapping, and found that this did not eliminate the observed reduction in the estimated Southern Ocean CO_2 sink. However, it may be that there are as yet undiscovered biases in the float data, which require ground-truthing and calibration against the more established shipboard measurements to ensure their accuracy. Furthermore, even assuming it is accurate, the float-derived pCO_2^{surf} can do nothing to improve historical coverage.

In this study, we present an alternative method of addressing the paucity of wintertime observations of pCO_2 in the Southern Ocean, based on the method of Nomura et al. (2014). By utilizing historical subsurface summertime observations from the Global Ocean Data Analysis Project (GLODAP, Olsen et al., 2019) v2.2019, we extrapolate new "pseudo observations" of wintertime pCO_2^{surf}. These pseudo observations add wintertime coverage in all sectors of the Southern Ocean. We then combine them with observations of pCO_2^{surf} from SOCAT version 2019 and use a multiple linear regression (MLR) to produce a gap-filled time-evolving map of pCO_2 from which we construct a new estimate of the air-sea CO_2 flux. In the next section, we describe how we have constructed and validated our pseudo observations, in Section 3 we describe the mapping, in Section 4 we explain our estimation of the air-sea flux, and in Sections 5 and 6 we present and discuss our results.

2. Pseudo Observations

2.1. Method

GLODAP contains profiles of various carbonate system parameters with depth, including DIC, Total Alkalinity (TA), as well as temperature (T) and salinity (S). Such observations were used by McNeil et al. (2007) to calculate pCO_2^{surf} and hence estimate the air-sea flux of CO_2. They have also be used by Nomura et al. (2014) to produce extrapolated estimates of pCO_2^{surf} in the wintertime of 2005 using summertime observations from the seasonal ice zone in the Indian Sector of the Southern Ocean, using the principle we now describe.

During winter, typically a deep mixed layer develops while the surface of the ocean cools and gases exchange with the atmosphere (Figure 2). During spring and summer the surface layer warms and restratifies, forming a pycnocline above the lower part of the winter mixed layer that isolates the winter water from the atmosphere. In the Southern Ocean south of the Polar Front, a temperature minimum layer (TML) forms because the winter surface water is cooler than both the summer surface layer above and the deeper waters below (Tomczak & Liefrink, 2005). Taking summertime profiles of temperature with depth from GLODAP, we can therefore use this TML to identify waters that were last in contact with the atmosphere during the previous winter. We make the assumption that the TML water is representative of surface conditions in Sep-

tember, regarding this as the end of winter before the surface layer begins to warm and restratify. We search for a TML in the GLODAP profiles in all non-winter months, defined as October to May, and we generate pseudo observations for all of these months. The vast majority of TML profiles (84%) are from December to March, and we have validated pseudo observations from these months in Section 2.2. We also find that excluding pseudo observations constructed from profiles in April to May, which have the longest gap since the previous winter, has a negligible impact on our air-sea CO_2 flux estimate (these pseudo observations are included in the results presented).

We identify the TML using the following procedure. Taking profiles of temperature, salinity, and pressure from each year of GLODAP, we remove observations where the pressure is >500 dbar, so as to limit our search for a TML to those waters that might reasonably have been part of a winter mixed layer. The summer mixed layer depth (MLD) is then identified as the depth at which the potential density increases above a given threshold, "MLDtol", compared to the surface, and we then seek a temperature minimum between this depth and 500 m, which we define as our TML. We find that an MLDtol of 0.03 kg m^{-3} gives MLDs that agree well with a MLD climatology from Holte et al. (2017) in terms of their mean seasonal cycle and the spatial pattern of the long term mean for our study region. We vary MLDtol between 0.02 and 0.04 kg m^{-3} in MonteCarlo ensembles which we use to explore the uncertainties on our air-sea CO_2 fluxes (see Section 4 and Table C1), but our results are not sensitive to this choice.

To check that we are correctly identifying the surface winter water in the TML, we compare the TML T and S values with September surface layer (top 10 m) T and S from a gridded Argo product (Roemmich & Gilson, 2009). We find the values are well correlated, with Pearson coefficients of 0.83 and 0.7, and root-mean-squared errors (RMSE) of 0.96°C and 0.16 PSU for T and S, respectively (note that inaccuracies in the gridded Argo product in poorly sampled regions, particularly in sea ice, contribute to the RMSE).

Having identified the TML, we obtain the concentration of DIC within that TML from GLODAP. This is then adjusted for the effects of biological activity that has occurred in the winter water since it was last in contact with the atmosphere. We make this adjustment by assuming a Redfield Ratio $RR_{C:O}$ between the change in DIC and the change in oxygen between winter and summer due to biological activity:

$$\Delta\mathrm{DIC}\,(winter \rightarrow summer) = \mathrm{RR}_{\mathrm{C:O}}\,\mathrm{AOU} \tag{1}$$

where AOU is the apparent oxygen utilization of the TML water, also from GLODAP, which is assumed to be the change in oxygen since the water was last ventilated in wintertime. To account for wintertime surface oxygen undersaturation in sea ice-covered regions we apply a correction to AOU of the form $\mathrm{AOU}^{\mathrm{corr}} = (1 - a\mathrm{C}_{\mathrm{ice}}{}^{b})\mathrm{AOU}$, where C_{ice} is the sea ice concentration from the NOAA/NSIDC product (Meier et al., 2017; Peng et al., 2013), and the values of "a" and "b" are established during the validation with SOCAT data described in the next section. We vary $RR_{C:O}$ between two possibilities, $\frac{106}{138}$ and $\frac{106}{150}$, which are classic and revised Redfield Ratios quoted in Sarmiento and Gruber (2013), in our MonteCarlo ensembles. We have ignored any spatial or temporal variability in $RR_{C:O}$.

In the previous paragraph, we have described a correction to AOU in the sea ice zone; however SOCCOM float data suggest that surface waters are undersaturated in oxygen over much of our study region in winter (Bushinsky, Gray, et al., 2017). Based on our analysis of the same float data, we apply a uniform correction of −13.5 μmol kg^{-1} to AOU used in the construction of pseudo observations in the region between the Polar Front and the sea ice. We find in the next section that this correction has a detrimental impact on our validation; however, we have applied it on the grounds that it is likely needed to remove a known bias. It may be that a spatially (and perhaps temporally) varying AOU correction would reconcile the discrepancies, but this would only be feasible for the most recent years since the deployment of the biogeochemical floats, and we will leave it for future work.

In order to create pseudo observations of $\mathrm{pCO}_2{}^{\mathrm{surf}}$ from our wintertime pseudo DIC, we have used MATLAB CO2SYS software (van Heuven et al., 2011) as follows. We calculate TA using a locally interpolated alkalinity regression for global alkalinity estimation (LIAR, Carter et al., 2016) with inputs of T and S from a time-varying gridded Argo product (Roemmich & Gilson, 2009) and of silicate (Si), oxygen (O) and ni-

trate (Ni) from the GLODAP gridded climatology. We use dissociation constants of Millero et al. (2006), Dickson (1990), and Lee et al. (2010), and finally combine the DIC, TA, Argo T and S, and GLODAP Si and phosphate (P) to calculate pCO_2 using CO2SYS. We take a mean over a surface layer, varied between 5 and 20 m in MonteCarlo ensembles, of the DIC, TA, T and S input to CO2SYS to produce our pseudo observations of pCO_2^{surf}; for Si and P we have used fixed values (see Table C1). In converting our pseudo observations of DIC to pCO_2^{surf} in this manner, and in applying the AOU correction due to sea ice detailed above, we have assumed that our pseudo DIC from a summertime TML at a depth of between ∼50 and ∼200 m (see Figure A1) is representative of the surface DIC in the previous September within the same 1° latitude by 1° longitude box. This assumption excludes the possibility of horizontal transports and mixing having altered the properties of the TML over time, and we are not able to correct for this; however the validation we show in the next section gives us confidence that these effects are not important.

2.2. Validation

Where possible, we have validated our wintertime pseudo observations of DIC using real wintertime observations, also from GLODAP. For this validation, there is only one year (1998) in the GLODAP data set for which there exist summertime observations south of the polar front in the same region as wintertime observations the previous winter (Figure 3a). To provide additional validation, we have also compared pseudo DIC from 2005 along a section in Drake Passage with observed DIC from 2009 (Figure 3b). We have corrected the 2005 pseudo observations for an increase of 3 μmol kg^{-1} in DIC between 2005 and 2009 due to the increase in atmospheric CO_2. The correction was estimated by first taking a mean of the atmospheric CO_2 mole fraction from the NOAA marine boundary layer product (Dlugokencky et al., 2017) between 64.5°S and 35.5°S, which changes from 375.3 in 2005 to 383.4 in 2009. We then plug these values into CO2SYS with constant values of $TA = 2{,}380$ μmol kg^{-1}, $T = -0.4$°C and $S = 34$ PSU to obtain the average change in DIC. This estimate does not account for the possibility of spatial variations in the surface DIC trend, which may be weak or even negative locally. We compare annual means (Figure 3c) rather than individual observations because the real and pseudo observations are not collocated; however, there is good agreement at a more granular level as well, as can be seen on Figure 3b. On the means, the difference between the pseudo and observed DIC is 7.1 μmol kg^{-1} for 1998 and 8.5 μmol kg^{-1} for 2005/2009. If we remove the −13.5 μmol kg^{-1} bias correction to AOU discussed in Section 2, the differences in the means are −3.3 μmol kg^{-1} for 1998 and 5.7 μmol kg^{-1} for 2005/2009.

We additionally validate our pseudo observations with collocated, contemporaneous observations from SOCAT. We identify SOCAT observations from the same month and year as a pseudo observation applies to, and which are located within ±1° latitude or longitude, and take a mean over the SOCAT observations to compare with that pseudo observation. We convert the SOCAT pCO_2 values to DIC and compare to our pseudo observations of DIC, thereby removing the effects of T and S on pCO_2 in the comparison. The conversion is done with CO2SYS, using inputs of T and S from SOCAT, assuming the same GLODAP climatological values of O, Si and Ni as were used to construct the pseudo pCO_2, and estimating alkalinity using LIAR applied to those T, S, O, Si, and Ni (the climatological uncertainties on the latter three variables have negligible effect on this calculation). We convert each SOCAT observation collocated with a pseudo observation to DIC before taking a mean.

For the whole study period, there are 17 pseudo observations, from the years 2005 and 2008, for which there exist SOCAT observations for validation, and they are all in Drake Passage (Figure 4a). We find that overall agreement is good, with the pseudo observations slightly overestimating DIC compared with the 2005 SOCAT observations (Figure 4b), and slightly underestimating it compared with those from 2008 (Figure 4c). The RMSE and bias for both years combined are 13.9 and 4.1 μmol kg^{-1}, respectively. This reduces to 12.3 and 1.1 μmol kg^{-1} if we remove the AOU bias correction away from the sea ice. If we compare pCO_2 instead of DIC (Figure B1), the RMSE and bias are 39.9 and 10.8 μatm, respectively. These reduce to 34.1 and 5.5 μatm without the AOU bias correction. While the bias correction has worsened the agreement between our pseudo observations and both the GLODAP and SOCAT observations we have used for validation, we will account for this by covering the range of AOU uncertainty in our MonteCarlo ensembles (see Section 4).

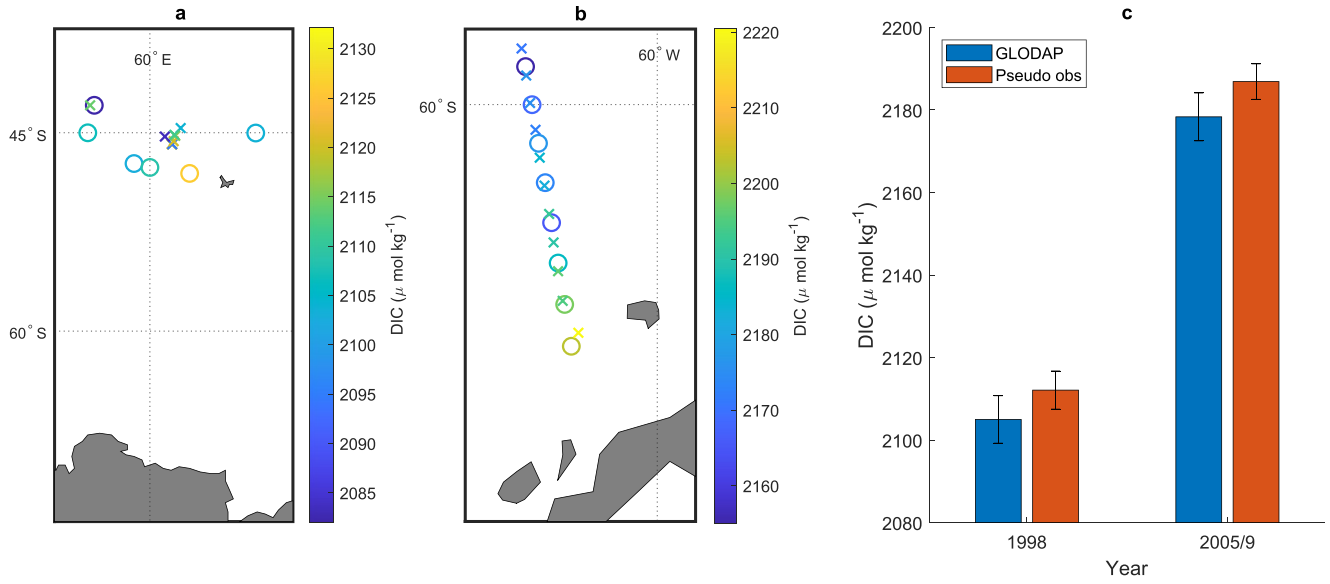

Figure 3. Validation of pseudo observations against in situ surface layer winter DIC observations from GLODAP. Panel (a) is a map showing pseudo (crosses) and real (circles) observations of DIC in the year 1998, with the Antarctic continent to the south. Panel (b) is a map showing pseudo observations in 2005 (crosses) and real observations DIC in 2009 (circles) for the section north of the Antarctic peninsula. Panel (c) compares the means of the real and pseudo observations shown on (a and b), with the error bars showing the standard error on the mean.

There are some discrepancies between the individual pseudo observations and SOCAT. A possible explanation for the apparent underestimate by our pseudo observations in the two most southerly 2008 stations (Figure 4c) lies with the sea ice concentrations. The horizontal gradient in the sea ice concentration in the region of these stations in September 2008 is strong, and the concentration is locally decreasing southwards. If the concentrations are underestimated due to the resolution of the sea ice product, then that would bias our pseudo observations low. On the 2005 transect, the most northerly pseudo observations are overestimat-

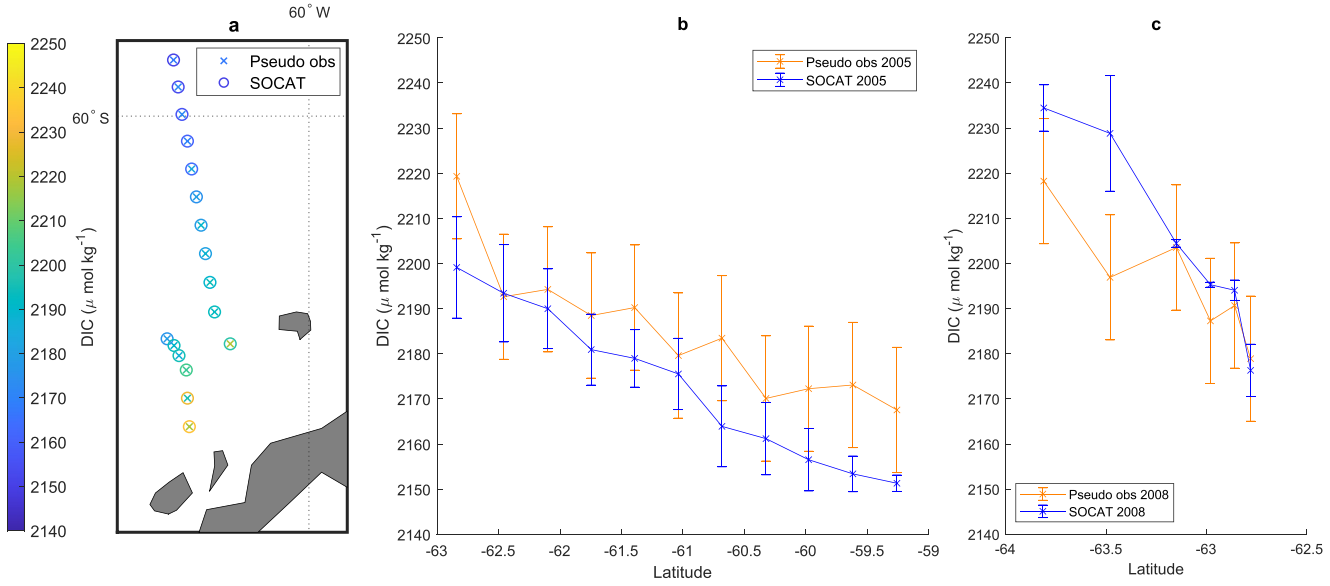

Figure 4. Validation of pseudo observations against SOCAT. Panel (a) is a map showing pseudo observations (crosses) and means of collocated contemporaneous real observations (circles) north of the Antarctic peninsula. Panels (b and c) show the same observations plotted against latitude for 2005 and 2008, respectively, with pseudo observations in orange and real observations in blue. The error bars on the SOCAT observations are the standard deviations of the individual observations contributing to the mean for each point; the error bars on the pseudo observations show the overall RMS error between the pseudo and SOCAT observations. The SOCAT pCO_2 values were converted to DIC (see Section 2.2); a similar plot but showing pCO_2 is in Appendix B.

ed compared with SOCAT. These stations are in the region between the sea ice and the Polar Front where a bias correction has been applied to the AOU involved in the pseudo observations calculation; with this correction removed the four most northerly SOCAT observations fall within the error bars of the pseudo observations. Two further pseudo observations in 2005, one at around 60.7°S and one at 62.8°S, stand out as overestimates compared with SOCAT (the discrepancy is more obvious in the pCO_2 comparison shown on Figure B1). These pseudo observations derive from summer profiles where the temperature minimum was at 150 and 200 dbar, much deeper than the ∼70 dbar for the majority of the TML profiles in that year (2005, see Figure A1). However, the temperature profiles do still have a characteristic TML shape. We suggest that these deep temperature minima result from localized, short-lived deep winter mixing events which entrain deeper waters rich in natural carbon and thus produce pseudo observations with high values of DIC and pCO_2. If these events did not occur at the right time to coincide with the validating SOCAT observations, this would explain the overestimate.

We use the comparison with SOCAT to establish optimized values of the parameters "a" and "b" used to correct the AOU in sea ice-covered regions. We explored a range of values for both parameters, creating sets of pseudo observations and calculating the RMSE for all 17 stations on Figure 4 for each set. The parameters that give the best fit are $a = 0.9$ and $b = 0.3$, with RMSE = 13.9 μmol kg^{-1}. The same optimization carried out using the pCO_2 values shown in Figure B1 results in the same best fit parameters, and an RMSE = 39.9 μatm.

3. pCO_2 Mapping

Having created pseudo observations that improve wintertime coverage of observed pCO_2 in the Southern Ocean south of the Polar Front (Figure 1), the next step is to use the available observations to map pCO_2^{surf} in space and time, as with the studies referred to in Section 1. We use a simple MLR, which while unable to fit the observations as closely as more complex methods such as the neural network approach of Landschützer, Gruber, Bakker, Schuster, et al. (2013), has the advantages of simplicity and modest computation requirements, allowing us to carry out our MonteCarlo ensembles to explore uncertainty. The variables on which we base the MLR are the atmospheric CO_2 mole fraction xCO_2^{atm}, T, S, and MLD. pCO_2^{surf} depends directly on T and S, and indirectly on MLD because surface mixing entrains DIC into the mixed layer from below. Including xCO_2^{atm} allows us to capture some of the interannual variability and the trend, however, as we will see later the former tends to be underestimated by this method. T and S have the advantage, thanks to the Argo program, that they are comparatively well known in time and space.

We use the Roemmich-Gilson (R-G) Argo product in which T and S are gridded with 1° horizontal resolution, on 58 depth levels (34 in the top 500 m), and with monthly values for our study period. We obtain xCO_2^{atm} from the NOAA marine boundary layer product (Dlugokencky et al., 2017), also with monthly values on a 1° × 1° grid. We obtain MLDs from the monthly climatology of Holte et al. (2017), which applies an algorithm to density profiles based on Argo data, also on a 1° × 1° grid. The MLD algorithm has proven more accurate than threshold methods, which tend to overestimate MLDs particularly in polar regions (Holte & Talley, 2009). We apply the same climatology to every year, thereby neglecting any interannual variability in MLD. There are gaps in the climatology which we fill by trilinear interpolation of the fields (dimensions of latitude, longitude, and month). We also tested filling the gaps with MLD values derived from a density threshold method applied to the R-G Argo product gridded T and S fields, and this gives nearly identical results.

In addition to our pseudo observations, we calculate pCO_2^{surf} directly from GLODAP observations, and we also take it from a gridded version of SOCAT. The GLODAP pCO_2^{surf} is constructed by calculating profiles of pCO_2 using CO2SYS on GLODAP profiles of DIC, TA, T, and S, and using the same Si and P as for the pseudo observations, and averaging those pCO_2 profiles over the 10 m surface layer. All three sets of observations (pseudo, GLODAP, and SOCAT) are combined and regressed on their associated T, S, MLD and year, to produce a time-evolving map of pCO_2^{surf}. In the regression, each grid point from the SOCAT product containing a pCO_2^{surf} value is counted as a single observation, as is each individual pseudo observation and each GLODAP-derived pCO_2^{surf} observation. We associate the pseudo observations with the

their nearest gridded Argo T and S values from September of the relevant year, averaged over the surface layer, and similarly with MLDs from the Holte et al. (2017) climatology. In the case of pCO_2^{surf} derived directly from GLODAP observations, the T and S is taken from the GLODAP profiles, again averaged over the surface layer, and the MLD is obtained from the climatology. In the case of the SOCAT gridded pCO_2^{surf}, T and S comes from the SOCAT product and MLD from the climatology. In all cases xCO_2^{atm} is taken from the nearest latitude/longitude grid cell to the pseudo, GLODAP or SOCAT observation in the relevant month and year.

Finally, before calculating the MLR we split the observations into two regions, one north and one south of the mean position of the Polar Front. This is a simplification of the approach used by Landschützer, Gruber, Bakker, Schuster, et al. (2013) and others, where the ocean is split into biogeochemical provinces, or "biomes"; in our case since we have relatively few pseudo observations (760), if we were to use similar biomes there would be several that contained no pseudo observations. Therefore, we split only at the Polar Front on the grounds that the pseudo observations can only be calculated to its south. We carry out the MLR both with and without the pseudo observations included in the data set, so as to determine their impact. We validated the MLR mapping by comparing the mapped gridded pCO_2^{surf} with the nearest in situ observations from the entire SOCAT database in the same month and year, obtaining an RMSE of 24.5 μatm. These observations are not independent of the mapping because they are the basis on which the SOCAT gridded values we include in our MLR are constructed, but this validation gives an indication of how well we are fitting the data.

4. CO_2 Flux Calculation

We calculate the air-sea flux of CO_2 from the difference between pCO_2^{surf} and the atmospheric pCO_2^{atm}, according to the formula:

$$F_{CO2} = (1 - C_{ice})kK_0(pCO_2^{surf} - pCO_2^{atm}). \quad (2)$$

In Equation 2, k is the gas transfer velocity calculated according to Nightingale et al. (2000) and using CCMP 6-hourly winds (Atlas et al., 2011) and sea surface temperature from the surface layer of the R-G gridded Argo product, and K_0 is the solubility calculated according to Weiss (1974) and using sea surface temperature and sea surface salinity from the gridded Argo product. pCO_2^{atm} was calculated from xCO_2^{atm} following Cooper et al. (1998) and using gridded Argo sea surface temperature and NCEP/NCAR sea level pressure (Kalnay et al., 1996).

Uncertainty on F_{CO2} comes from a number of sources, which we describe here, and summarize in Table C1. Each of the parameters and errors identified are varied in a 200-member MonteCarlo ensemble to estimate the envelope of uncertainty on F_{CO2}, and we also give the range of parameters explored in Table C1.

The GLODAP AOU used to adjust our pseudo DIC for biological activity between winter and summer may be overestimated because of wintertime undersaturation of surface oxygen (ΔO_2) in some regions. We assign normally distributed random errors to AOU with a mean of −13.5 μmol kg^{-1} and a standard deviation of 15 μmol kg^{-1} away from sea ice, and normally distributed random errors with a mean of zero and a standard deviation of 15 μmol kg^{-1} in sea ice (where the AOU correction described in Section 2 based on sea ice concentration has also been applied). The normally distributed errors are designed to cover the range of likely ΔO_2 values that would necessitate a correction to AOU. Between the Polar Front and the sea ice zone the $\pm 1\sigma$ range is between −28.5 and +1.5 μmol kg^{-1}, and in the sea ice zone it is between ∼−56 and ∼−26 μmol kg^{-1} (the latter range is a crude estimate based on the effect of our sea ice-based correction on typical TML AOU values of ∼54 μmol kg^{-1} found in the GLODAP data and mean September sea ice concentration of 0.56 within the region of >0 sea ice concentration).

Values of T and S from the R-G gridded Argo product are used in multiple parts of the method: in the construction of pseudo observations through (1) the LIAR TA estimation and (2) the calculation of pCO_2^{surf} using CO2SYS; (3) in the MLR mapping of pCO_2^{surf}; and in the calculation of (4) k and (5) K_0 used in estimating the air-sea CO_2 flux. Throughout we generate normally distributed random errors on T and S with

a mean of zero and allow them to propagate, but in (1 and 2) we use standard deviations for the normal distributions based on the comparison of TML with surface Argo *T* and *S* from Section 2, whereas in (3–5) we use more modest estimates of the uncertainty (see Table C1).

The MLDs from Holte et al. (2017) have relatively large uncertainties and contribute significantly to the uncertainty on the flux. At each grid point in the MLD climatology, we use the standard error of the MLDs contributing to the climatological mean at that point as the standard deviation for a normal distribution of random errors applied to the MLD.

We vary between 5 and 20 m the depth of the surface layer over which we average the various quantities used to calculate pCO_2^{surf} in our MonteCarlo ensemble. We establish bounds on the values of silicate and phosphate input to CO2SYS by taking a mean over our study region of the upper and lower bounds of those parameters in the GLODAP climatology, and vary them between their upper, mean, and lower bounds. We also investigated the impact of varying the GLODAP climatological silicate, oxygen, and nitrate fields input to LIAR for estimating TA for the pseudo observations. Varying these inputs within the climatological uncertainties has a negligible effect on our results, and they are kept constant in our ensembles. Finally, we generate a normal distribution of multipliers for the gas transfer coefficient *k* to simulate an uncertainty of 20% on this parameter.

5. Results

South of the Polar Front and north of the seasonal ice zone, the annual mean F_{CO2} is generally out of the ocean on the eastern side of Antarctica and into the ocean on the western side (Figures 5a and 5b). Within the seasonal ice zone the annual flux is generally into the ocean, but small. The addition of the pseudo observations has increased the outgassing in all sectors of the ACC, most strongly near the edge of the seasonal ice zone around 60°E (Figure 5c). In winter, there is outgassing around most of the ACC between the Polar Front and the seasonal ice zone, and very little flux within the seasonal ice zone as expected (Figures 5d and 5e). The impact on the winter mean of including the pseudo observations follows a similar spatial pattern as for the annual mean, but is larger in magnitude (Figure 5f; note that the color scale in subplots c and f differs from the rest). Nomura et al. (2014) reported sea-air flux densities of −0.4 mol C yr^{-1} m^{-2} in the seasonal ice zone between 32°E-58°E and 64°S-67°S for the winter of 2005. At those longitudes our estimate shows negligible flux at the extreme southern edge of our domain, which just overlaps with the northern extent of theirs.

The 2004–2017 mean seasonal cycle of F_{CO2} integrated over the region south of the Polar Front with the inclusion of the pseudo observations shows stronger outgassing/weaker uptake compared with that without pseudo observations (Figure 6a). We find a peak outgassing in July of 0.14 Pg C yr^{-1} (lower bound, upper bound 0.11, 0.17 Pg C yr^{-1}) with the pseudo observations, and 0.04 (0.03, 0.05) Pg C yr^{-1} without. The overall annual mean flux is −0.02 (−0.04, −0.00) Pg C yr^{-1} with the pseudo observations, and −0.09 (−0.10, −0.09) Pg C yr^{-1} without. Compared to flux estimates based on the pCO_2^{surf} products of R2013 (green dashed line), B2019 (dark red dashed line), and Landschützer, Gruber, and Bakker (2017) (bright red dashed line, hereafter L2017), our results exhibit a slightly weaker seasonal cycle, rather similar in shape to the L2017 estimate. Note that the flux estimates presented on Figure 6 from our methodology and from those of R2013, B2019, and L2017 are exactly comparable, in the sense that we have calculated F_{CO2} using the mapped pCO_2^{surf} from those studies combined with the same parameters in Equation 2 as we have used for our estimates, and integrated them over the same spatial domain and time period.

Over the course of the 2004–2017 time period studied, our estimated annual mean F_{CO2} south of the Polar Front has changed from a small source to a small sink (Figure 6b). With the pseudo observations included, our estimate goes from 0.12 (0.09, 0.14) Pg C yr^{-1} in 2004 to −0.14 (−0.15, −0.12) Pg C yr^{-1} in 2017, a trend of −0.19 Pg C yr^{-1} $decade^{-1}$. Without the pseudo observations, our estimate goes from 0.01 (0.00, 0.01) Pg C yr^{-1} in 2004 to −0.16 (−0.17, −0.16) Pg C yr^{-1} in 2017, a trend of −0.13 Pg C yr^{-1} $decade^{-1}$. The estimate with pseudo observations is 0.12 Pg C yr^{-1} above that without in 2004, and the two estimates gradually converge, almost overlapping by 2017.

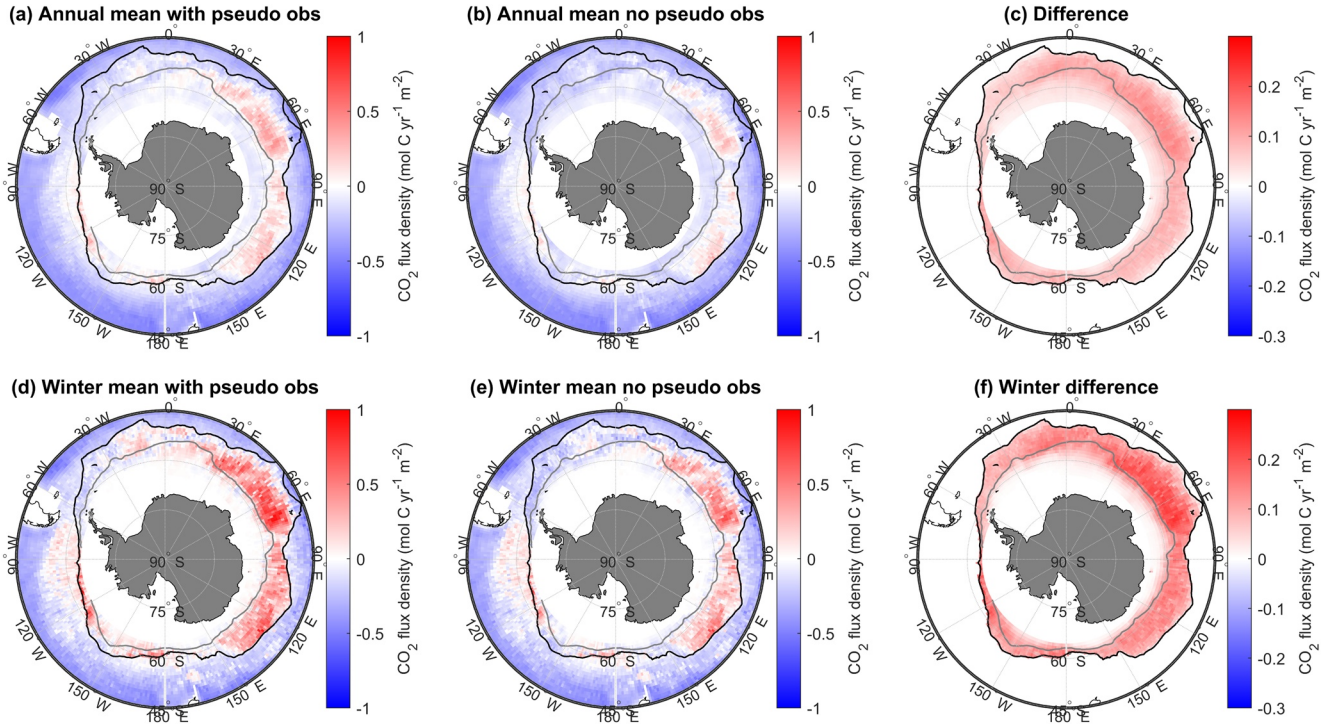

Figure 5. 2004–2017 mean sea-air CO_2 flux densities (negative fluxes are into the ocean). Results are shown with (a and d) and without (b and e) the inclusion of pseudo observations in the multiple linear regression, and the difference ($c = a - b, f = d - e$). Note the different color scales for the difference plots. Panels (a–c) show the annual mean; panels (d–f) the wintertime mean (June to September). The black line is the mean position of the Polar Front; the gray line the mean September ice extent (15% concentration contour). Note that the region south of 65°S is blank because this is the southerly limit of the Argo product on which we have based the MLR.

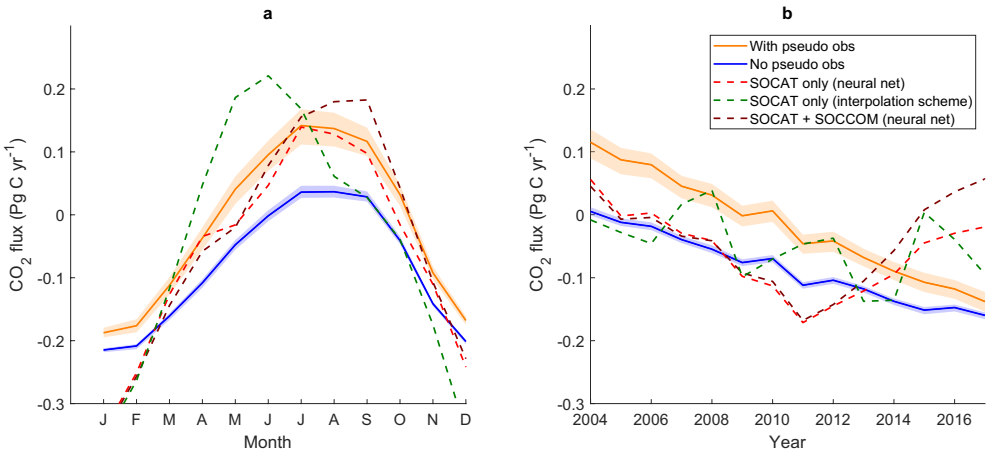

Figure 6. (a) 2004–2017 mean seasonal cycle and (b) annual means of F_{CO2} south of the Polar Front. The solid orange and blue lines are our estimates including and excluding the pseudo observations, respectively. The shaded areas give the 90% confidence bounds from our MonteCarlo ensemble. The dashed lines are estimates of F_{CO2} based on pCO_2^{surf} estimates from other studies, but otherwise calculated identically to our estimates and covering the same spatial/temporal domain. The bright red line is based on pCO_2^{surf} from Landschützer, Gruber, and Bakker (2017) which applied a neural network technique to SOCAT data. The green line is based on pCO_2^{surf} which used the interpolation method of Rödenbeck, Keeling, et al. (2013), also applied to SOCAT data. The dark red line is based on pCO_2^{surf} from Bushinsky, Landschützer, et al. (2019) which applied the Landschützer neural network technique to a combination of SOCAT and SOCCOM data.

Compared to the estimates based on R2013, B2019, and L2017, our estimate without pseudo observations follows the general trend between 2004 and ~2013 but with less variability, while the estimate with pseudo observations has a steeper downward trend. After 2013 the estimates based on other studies trend upwards while our results continue to follow the downward trend. The B2019 estimate (dark red dashed line) includes the use of SOCCOM float data from 2014, and this also has an influence on previous years which diminishes going back in time. This accounts for some of the strong upward trend, but the R2013 and L2017 estimates are based solely on SOCAT data, and they also trend upwards, by contrast to our results. Part of this discrepancy can be explained by the differences in gap-filling methods: we have used an MLR, which is constrained toward linearity and cannot reproduce the sharp change in trend captured by the more sophisticated techniques. If we split our MLR into two halves, training it first on the data from 2004 to 2011 and then from 2011 to 2017, we see an upward trend with the pseudo observations from 2011, that is still weaker than the estimates based on L2017 and B2019, but that overlaps with R2013 in 2017 (Figure D1). The upward trend in the later period is slightly stronger with the pseudo observations than without. In the earlier period, the outgassing is stronger, the difference due to the pseudo observations is more pronounced, and the downward trend is steeper compared with the estimates based on B2019 and L2017. In this period, our estimate without pseudo observations quite closely follows the trends of L2017 and B2019. We discuss the differences between our results and those based on comparable earlier studies further in the next section.

6. Discussion

We have found that the addition of wintertime pseudo observations of pCO_2^{surf} increased the strength of winter outgassing in estimates of the 2004–2017 mean seasonal cycle of air-sea CO_2 flux south of the Polar Front in the Southern Ocean. The pseudo observations also increased the weak annual mean outgassing at the beginning of the period, but the estimates with and without pseudo observations nearly converged in later years. Our results with pseudo observations show stronger outgassing/weaker uptake and a stronger downward trend compared with fluxes calculated from earlier estimates of pCO_2^{surf} between 2004 and 2013, and do not replicate the strength of a reversal of the trend to a reducing sink/becoming a source between 2013 and 2017 suggested by other studies.

The downward trend (increased uptake) in the annual mean flux from 2004 to 2017 seen in our estimates on Figure 6b is expected given the steady increase in atmospheric CO_2 concentrations over the same period; however it is at odds with other estimates based on pCO_2^{surf} reconstructed using more sophisticated techniques, which suggest a reversal of the downward trend in the latter part of the period. Because our estimates are constrained toward linearity by the linear nature of the MLR, we have tested the impact of splitting the MLR in two at 2011. We find that this does reproduce some of the upward trend, but it is weaker at least than that of fluxes based on pCO_2^{surf} reconstructions of L2017 and B2019. These estimates both used the neural network technique of Landschützer, Gruber, Bakker, Schuster, et al. (2013) for the reconstructions, but the former is based soley on SOCAT pCO_2^{surf} data and the latter includes data from SOCCOM floats. Another potential limitation to our method is that we have used a MLD climatology, which means that our F_{CO2} estimate is not influenced by interannual variability or trends in the MLDs. However, we find no obvious trend in MLDs estimated from the R-G gridded Argo product that would explain the upward trend in F_{CO2} suggested by other products.

Although the wintertime spatial coverage is much improved by the pseudo observations (Figure 1), the total number of grid points (lat/lon/month/year) occupied is still small: 760 compared with 27,983 from SOCAT. We tested the impact on our F_{CO2} estimates of artificially inflating the number of pseudo observations by simply including multiple copies of each pseudo observation in the data used in the MLR. We calculated F_{CO2} with up to 30 copies of the pseudo observations, such that they would be as numerous as the SOCAT observations. We find that increasing the influence of the pseudo observations increases the strength of the downward trend in the flux, therefore we conclude that they have not been swamped by the more numerous direct observations of pCO_2^{surf}. Of our 760 pseudo observations, 42 correspond to the year 2015, 8 to 2016, and 64 to 2017; these therefore must influence our flux estimates for the later years.

The largest difference was found between our estimates and one based on a neural network reconstruction of pCO_2^{surf} from B2019 including SOCCOM data, in the years 2015–2017 when the float data have the most influence. We attempt a comparison between our pseudo observations and SOCCOM float-derived DIC, and are able to locate three examples of pseudo observations in the same month and year and within ±2° latitude or longitude of a SOCCOM float with derived DIC observations. For these three, the DIC of the pseudo observations is on average only 2.0 μmol kg^{-1} lower than the comparable SOCCOM float values; however, this is a very small number of observations from which to draw inferences from the comparison. B2019 also investigated the effect of a possible bias in the float-derived pCO_2^{surf} by subtracting a uniform value of 4 μatm from their estimate, concluding that a mean bias of that magnitude would not account for the difference made by the float data to the CO_2 flux. However, it may be that such a uniform correction does not account for a bias that is unevenly distributed, or for a larger bias as yet unidentified. Our results reinforce the suggestion made by B2019 that more work may be needed to determine the accuracy of float-derived pCO_2^{surf}.

The seasonal cycle of our estimated CO_2 flux south of the Polar Front (Figure 6a), with its low in January and high in July, is very similar to the seasonal cycle of the mean MLD for the same region, suggesting the MLD is a key driver. By contrast, the seasonal cycle of the mean surface temperature is out of phase, having its low in September and high in February. The seasonal cycle of the surface salinity, which is linked to pCO_2^{surf} through its relationship to alkalinity, is almost in phase with the CO_2 flux, with a low in February and a high in September. Gregor et al. (2018) conclude that winter variability of pCO_2^{surf} in the Southern Ocean is driven by stratification and mixing, whereas summer variability is driven by primary production. They also find MLD to be the dominant predictor of winter pCO_2^{surf}, consistent with our results. This dependence on MLD has been linked to the entrainment of DIC-rich deep waters in wintertime (Lenton et al., 2013). During our validation we found that pseudo observations with anomalously high DIC were derived from summer profiles with particularly deep TMLs, suggesting that isolated deep winter mixing events might be important for observed winter outgassing.

We have presented a novel estimate of the air-sea flux of CO_2 in the Southern Ocean south of the Polar Front that utilizes summertime subsurface observations of carbonate system parameters to boost the wintertime coverage of pCO_2^{surf} data which are required to estimate the flux. We find that these additional pseudo observations of pCO_2^{surf} result in an increase in the estimated winter outgassing in the region, but that this increase is largest for the mid 2000s, and reduces with time. In 2017, the most recent year of our analysis, we estimate a CO_2 flux of −0.14 Pg C yr^{-1} (lower bound, upper bound −0.16, −0.12 Pg C yr^{-1}), which increases to −0.08 (−0.10, −0.05) Pg C yr^{-1} when the MLR is carried out separately on 2011–2017 data. This compares with +0.06 Pg C yr^{-1} derived from pCO_2^{surf} constructed using a neural network technique applied to a combination of data from ships and autonomous profiling floats. The difference is comparatively small, but it is significant that improving winter coverage does not bring our estimate in line with one which used the float data, so the origin of the discrepancy between shipboard and float data in the Southern Ocean winter remains unsolved. This is important because placing constraints on the Southern Ocean air-sea CO_2 flux and determining its variability is critical to our understanding of the global carbon cycle, and hence to our ability to make accurate climate projections.

Appendix A: TML Identification

Figure A1 shows some examples of TML profiles identified from the GLODAP data from a selection of years.

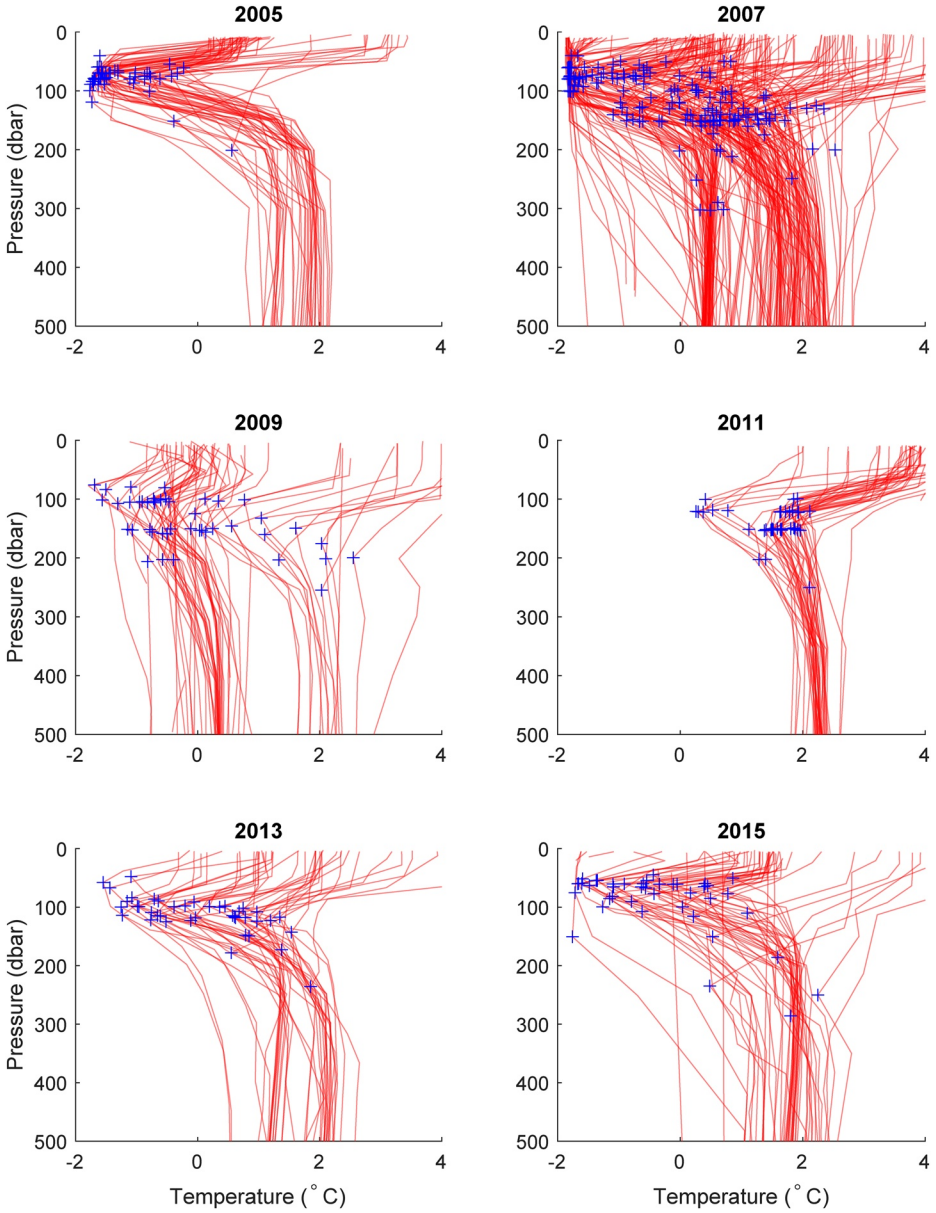

Figure A1. Identification of the Temperature Minimum Layer (TML) from GLODAP data. Red lines are the temperature profiles for all stations south of the polar front in a given year, and blue crosses show the location of the TML.

Appendix B: Validation of Pseudo Observations

Figure B1 shows the equivalent of Figure 4 validating the pseudo observations against SOCAT but comparing pCO_2 values instead of DIC.

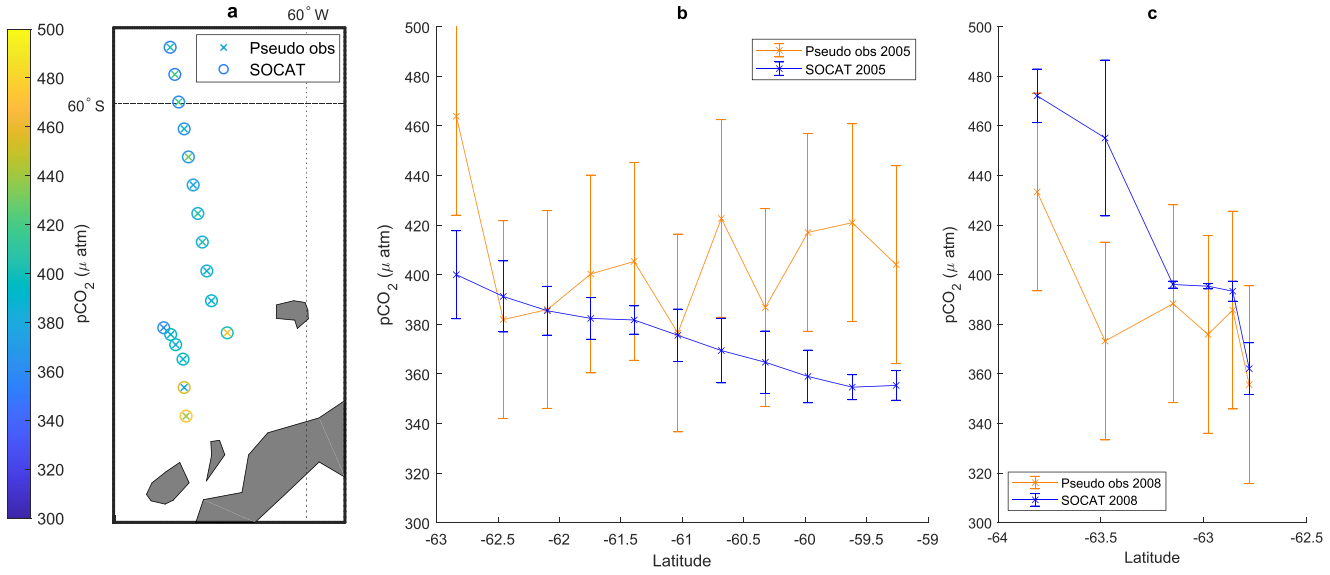

Figure B1. Validation of pseudo observations against SOCAT, as Figure 4 but showing pCO_2. Panel (a) is a map showing pseudo observations (crosses) and means of collocated contemporaneous real observations (circles) north of the Antarctic peninsula. Panels (b and c) show the same observations plotted against latitude for 2005 and 2008, respectively, with pseudo observations in orange and real observations in blue. The error bars on the SOCAT observations are the standard deviations of the individual observations contributing to the mean for each point; the error bars on the pseudo observations show the overall RMS error between the pseudo and SOCAT observations.

Appendix C: MonteCarlo Ensemble Parameters

Table C1 summarizes the range of parameters varied in the MonteCarlo ensemble to estimate the uncertainty on F_{CO2}.

Table C1
Range of Parameters Varied in MonteCarlo Ensemble to Estimate F_{CO2} *Uncertainty Envelope*

Parameter description	Values
AOU for adjusting pseudo obs DIC in sea ice (μmol kg^{-1})	Normally distributed random errors, mean 0, standard deviation 15
AOU for adjusting pseudo obs DIC away from sea ice (μmol kg^{-1})	Normally distributed random errors, mean −13.5, standard deviation 15
Redfield Ratio "$RR_{C:O}$"	$\frac{106}{138}, \frac{106}{150}$
R-G Argo *T* used for pseudo observations (°C)	Normally distributed random errors, mean 0, standard deviation 1
R-G Argo *S* used for pseudo observations (PSU)	Normally distributed random errors, mean 0, standard deviation 0.2
Assumed depth of surface layer (m)	5, 10, 20
Silicate input to CO2SYS (μmol kg^{-1})	10.0, 11.4, 12.8
Phosphate input to CO2SYS (μmol kg^{-1})	0.93, 0.98, 1.03
R-G Argo *T* used for mapping and flux calculation (°C)	Normally distributed random errors, mean 0, standard deviation 0.1
R-G Argo *S* used for mapping and flux calculation (PSU)	Normally distributed random errors, mean 0, standard deviation 0.0025
Climatological mixed layer depths	Normally distributed random errors, mean 0, standard deviation from MLD climatology
Density threshold for MLD identification (kg m^{-3})	0.02, 0.03, 0.04
Gas transfer velocity "*k*"	Normally distributed multiplier, mean 1, standard deviation 0.2

Appendix D: Air-Sea CO Fluxes

Figure D1 shows the equivalent of Figure 6b, where in this case our MLR was carried out separately on data from 2004 to 2011 and from 2011 to 2017.

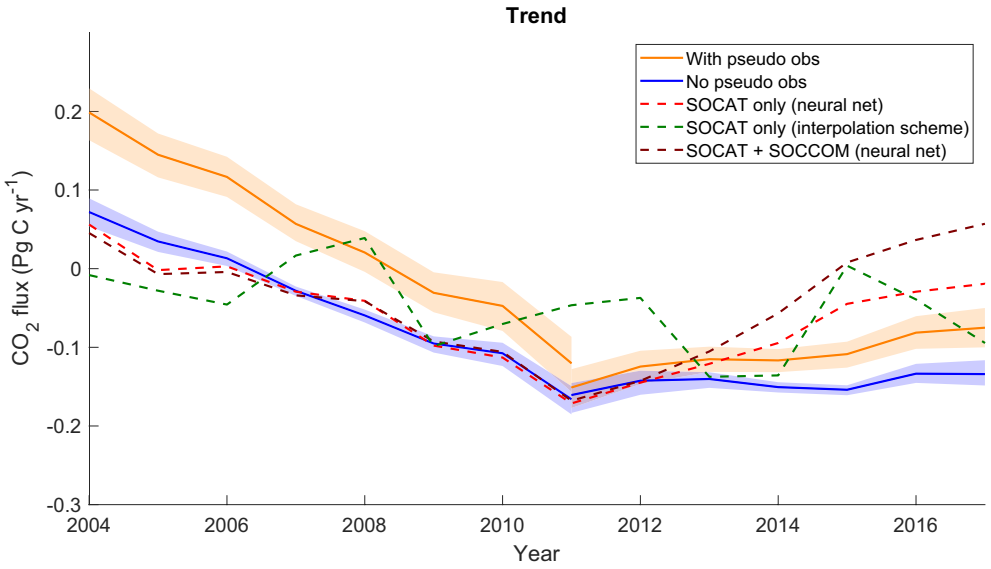

Figure D1. 2004–2017 annual means of F_{CO2} south of the Polar Front. As Figure 6b except the MLR has been carried out separately between 2004–2011 and 2011–2017. The solid orange and blue lines are our estimates including and excluding the pseudo observations, respectively. The shaded areas give the 90% confidence bounds from our MonteCarlo ensemble. The dashed lines are estimates of F_{CO2} based on pCO_2^{surf} estimates of Landschützer, Gruber, and Bakker (2017) (bright red line), Rödenbeck, Keeling, et al. (2013) (green line) and Bushinsky, Landschützer, et al. (2019) (dark red line).

Data Availability Statement

All of the data products used in this study are freely available online, links can be found through the following cited sources: Bakker et al. (2016), Olsen et al. (2019), Roemmich and Gilson (2009), Meier et al. (2017), Bushinsky, Gray, et al. (2017), Dlugokencky et al. (2017), Holte et al. (2017), Atlas et al. (2011), Kalnay et al. (1996), Rödenbeck, Keeling, et al. (2013), Bushinsky, Landschützer, et al. (2019), and Landschützer, Gruber, and Bakker (2017). CCMP Version-2.0 vector wind analyses are produced by Remote Sensing Systems; these data are available at www.remss.com. Argo data were collected and made freely available by the International Argo Program and the national programs that contribute to it (http://www.argo.ucsd.edu, http://argo.jcommops.org). The Argo Program is part of the Global Ocean Observing System (Argo 2000). Argo float data and metadata are from the Global Data Assembly Center (Argo GDAC, http://doi.org/10.17882/42182).

Acknowledgments
The authors acknowledge funding from the U.K. Natural Environment Research Council under the SONATA grant (NE/P021298/1). The authors also thank two anonymous reviewers for their constructive comments which have helped improve the paper.

References

Atlas, R., Hoffman, R. N., Ardizzone, J., Leidner, S. M., Jusem, J. C., Smith, D. K., & Gombos, D. (2011). A cross-calibrated, multiplatform ocean surface wind velocity product for meteorological and oceanographic applications. *Bulletin of the American Meteorological Society*, *92*(2), 157–174. https://doi.org/10.1175/2010BAMS2946.1

Bakker, D. C. E., Pfeil, B., Landa, C. S., Metzl, N., O'Brien, K. M., Olsen, A., et al. (2016). A multi-decade record of high-quality fCO_2 data in version 3 of the Surface Ocean CO_2 Atlas (SOCAT). *Earth System Science Data*, *8*(2), 383–413. https://doi.org/10.5194/essd-8-383-2016

Bushinsky, S. M., Gray, A. R., Johnson, K. S., & Sarmiento, J. L. (2017). Oxygen in the Southern Ocean from Argo floats: Determination of processes driving air-sea fluxes. *Journal of Geophysical Research: Oceans*, *122*(11), 8661–8682. https://doi.org/10.1002/2017JC012923

Bushinsky, S. M., Landschützer, P., Rödenbeck, C., Gray, A. R., Baker, D., Mazloff, M. R., et al. (2019). Reassessing Southern Ocean air-sea CO_2 flux estimates with the addition of biogeochemical float observations. *Global Biogeochemical Cycles*, *33*(11), 1370–1388. https://doi.org/10.1029/2019GB006176

Carter, B. R., Williams, N. L., Gray, A. R., & Feely, R. A. (2016). Locally interpolated alkalinity regression for global alkalinity estimation. *Limnology and Oceanography: Methods*, *14*(4), 268–277. https://doi.org/10.1002/lom3.10087

Cooper, D. J., Watson, A. J., & Ling, R. D. (1998). Variation of pCO_2 along a North Atlantic shipping route (U.K. to the Caribbean): A year of automated observations. *Marine Chemistry*, *60*(1–2), 147–164. https://doi.org/10.1016/S0304-4203(97)00082-0

Devries, T. (2014). The oceanic anthropogenic CO_2 sink: Storage, air-sea fluxes, and transports over the industrial era. *Global Biogeochemical Cycles*, *28*(7), 631–647. https://doi.org/10.1002/2013GB004739

Dickson, A. G. (1990). Thermodynamics of the dissociation of boric acid in potassium chloride solutions from 273.15 to 318.15 K. *Journal of Chemical & Engineering Data*, *35*(3), 253–257. https://doi.org/10.1021/je00061a009

Dlugokencky, E., Thoning, K., Land, P., & Tans, P. (2017). *NOAA greenhouse gas reference from atmospheric carbon dioxide dry air mole fractions from the NOAA ESRL carbon cycle cooperative global air sampling network*. Retrieved from ftp://aftp.cmdl.noaa.gov/data/trace_gases/co2/flask/surface/

Fay, A. R., McKinley, G. A., & Lovenduski, N. S. (2014). Southern Ocean carbon trends: Sensitivity to methods. *Geophysical Research Letters*, *41*(19), 6833–6840. https://doi.org/10.1002/2014GL061324

Freeman, N. M., & Lovenduski, N. S. (2016). Mapping the Antarctic Polar front: Weekly realizations from 2002 to 2014. *Earth System Science Data*, *8*(1), 191–198. https://doi.org/10.5194/essd-8-191-2016

Friedlingstein, P., Jones, M. W., O'Sullivan, M., Andrew, R. M., Hauck, J., Peters, G. P., et al. (2019). Global carbon budget 2019. *Earth System Science Data*, *11*(4), 1783–1838. https://doi.org/10.5194/essd-11-1783-2019

Frölicher, T. L., Sarmiento, J. L., Paynter, D. J., Dunne, J. P., Krasting, J. P., & Winton, M. (2015). Dominance of the Southern Ocean in anthropogenic carbon and heat uptake in CMIP5 models. *Journal of Climate*, *28*(2), 862–886. https://doi.org/10.1175/JCLI-D-14-00117.1

Gray, A. R., Johnson, K. S., Bushinsky, S. M., Riser, S. C., Russell, J. L., Talley, L. D., et al. (2018). Autonomous biogeochemical floats detect significant carbon dioxide outgassing in the high-latitude Southern Ocean. *Geophysical Research Letters*, *45*(17), 9049–9057. https://doi.org/10.1029/2018GL078013

Gregor, L., & Gruber, N. (2021). OceanSODA-ETHZ: A global gridded data set of the surface ocean carbonate system for seasonal to decadal studies of ocean acidification. *Earth System Science Data*, *13*(2), 777–808. https://doi.org/10.5194/essd-13-777-2021

Gregor, L., Kok, S., & Monteiro, P. M. S. (2017). Empirical methods for the estimation of Southern Ocean CO_2: Support vector and random forest regression. *Biogeosciences*, *14*(23), 5551–5569. https://doi.org/10.5194/bg-14-5551-2017

Gregor, L., Kok, S., & Monteiro, P. M. S. (2018). Interannual drivers of the seasonal cycle of CO_2 in the Southern Ocean. *Biogeosciences*, *15*(8), 2361–2378. https://doi.org/10.5194/bg-15-2361-2018

Gruber, N., Gloor, M., Mikaloff Fletcher, S. E., Doney, S. C., Dutkiewicz, S., Follows, M. J., et al. (2009). Oceanic sources, sinks, and transport of atmospheric CO_2. *Global Biogeochemical Cycles*, *23*(1). https://doi.org/10.1029/2008GB003349

Holte, J., & Talley, L. (2009). A new algorithm for finding mixed layer depths with applications to Argo data and Subantarctic Mode Water formation. *Journal of Atmospheric and Oceanic Technology*, *26*(9), 1920–1939. https://doi.org/10.1175/2009JTECHO543.1

Holte, J., Talley, L. D., Gilson, J., & Roemmich, D. (2017). An Argo mixed layer climatology and database. *Geophysical Research Letters*, *44*(11), 5618–5626. https://doi.org/10.1002/2017GL073426

Johnson, K. S., Plant, J. N., Coletti, L. J., Jannasch, H. W., Sakamoto, C. M., Riser, S. C., et al. (2017). Biogeochemical sensor performance in the SOCCOM profiling float array. *Journal of Geophysical Research: Oceans*, *122*(8), 6416–6436. https://doi.org/10.1002/2017JC012838

Kalnay, E., Kanamitsu, M., Kistler, R., Collins, W., Deaven, D., Gandin, L., et al. (1996). The NCEP/NCAR 40 yr reanalysis project. *Bulletin of the American Meteorological Society*, *77*(3), 437–471. https://doi.org/10.1175/1520-0477(1996)077⟨0437:TNYRP⟩2.0.CO;2

Landschützer, P., Gruber, N., & Bakker, D. C. (2017). *An observation-based global monthly gridded sea surface pCO_2 product from 1982 onward and its monthly climatology (NCEI Accession 0160558)*. NOAA National Centers for Environmental Information. Dataset. Retrieved from https://doi.org/10.7289/v5z899n6

Landschützer, P., Gruber, N., Bakker, D. C. E., & Schuster, U. (2014). Recent variability of the global ocean carbon sink. *Global Biogeochemical Cycles*, *28*(9), 927–949. https://doi.org/10.1002/2014GB004853

Landschützer, P., Gruber, N., Bakker, D. C. E., Schuster, U., Nakaoka, S., Payne, M. R., et al. (2013). A neural network-based estimate of the seasonal to interannual variability of the Atlantic Ocean carbon sink. *Biogeosciences*, *10*(11), 7793–7815. https://doi.org/10.5194/bg-10-7793-2013

Landschützer, P., Gruber, N., Bakker, D. C. E., Stemmler, I., & Six, K. D. (2018). Strengthening seasonal marine CO_2 variations due to increasing atmospheric CO_2. *Nature Climate Change*, *8*(2), 146–150. https://doi.org/10.1038/s41558-017-0057-x

Lee, K., Kim, T.-W., Byrne, R. H., Millero, F. J., Feely, R. A., & Liu, Y.-M. (2010). The universal ratio of boron to chlorinity for the North Pacific and North Atlantic oceans. *Geochimica et Cosmochimica Acta*, *74*(6), 1801–1811. https://doi.org/10.1016/j.gca.2009.12.027

Lenton, A., Tilbrook, B., Law, R. M., Bakker, D., Doney, S. C., Gruber, N., et al. (2013). Sea-air CO_2 fluxes in the Southern Ocean for the period 1990–2009. *Biogeosciences*, *10*(6), 4037–4054. https://doi.org/10.5194/bg-10-4037-2013

McNeil, B. I., Metzl, N., Key, R. M., Matear, R. J., & Corbiere, A. (2007). An empirical estimate of the Southern Ocean air-sea CO_2 flux. *Global Biogeochemical Cycles*, *21*(3). https://doi.org/10.1029/2007GB002991

Meier, W., Fettere, M. S., Mallory, R. D., & Stroeve, J. (2017). *NOAA/NSIDC climate data record of passive microwave sea ice concentration, version 3*. Retrieved from https://doi.org/10.7265/N59P2ZTG

Millero, F. J., Graham, T. B., Huang, F., Bustos-Serrano, H., & Pierrot, D. (2006). Dissociation constants of carbonic acid in seawater as a function of salinity and temperature. *Marine Chemistry*, *100*(1–2), 80–94. https://doi.org/10.1016/j.marchem.2005.12.001

Mongwe, N. P., Chang, N., & Monteiro, P. M. S. (2016). The seasonal cycle as a mode to diagnose biases in modeled CO_2 fluxes in the Southern Ocean. *Ocean Modelling*, *106*, 90–103. https://doi.org/10.1016/j.ocemod.2016.09.006

Mongwe, N. P., Vichi, M., & Monteiro, P. M. S. (2018). The seasonal cycle of pCO_2 and CO_2 fluxes in the Southern Ocean: Diagnosing anomalies in CMIP5 Earth system models. *Biogeosciences*, *15*(9), 2851–2872. https://doi.org/10.5194/bg-15-2851-2018

Nightingale, P. D., Malin, G., Law, C. S., Watson, A. J., Liss, P. S., Liddicoat, M. I., et al. (2000). In situ evaluation of air-sea gas exchange parameterizations using novel conservative and volatile tracers. *Global Biogeochemical Cycles*, *14*(1), 373–387. https://doi.org/10.1029/1999GB900091

Nomura, D., Yoshikawa-Inoue, H., Kobayashi, S., Nakaoka, S., Nakata, K., & Hashida, G. (2014). Winter-to-summer evolution of pCO_2 in surface water and air-sea CO_2 flux in the seasonal ice zone of the Southern Ocean. *Biogeosciences*, *11*(20), 5749–5761. https://doi.org/10.5194/bg-11-5749-2014

Olsen, A., Lange, N., Key, R. M., Tanhua, T., Álvarez, M., Becker, S., et al. (2019). GLODAPv2.2019 - An update of GLODAPv2. *Earth System Science Data*, *11*(3), 1437–1461. https://doi.org/10.5194/essd-11-1437-2019

Peng, G., Meier, W. N., Scott, D. J., & Savoie, M. H. (2013). A long-term and reproducible passive microwave sea ice concentration data record for climate studies and monitoring. *Earth System Science Data*, *5*(2), 311–318. https://doi.org/10.5194/essd-5-311-2013

Rödenbeck, C., Bakker, D. C. E., Gruber, N., Iida, Y., Jacobson, A. R., Jones, S., et al. (2015). Data-based estimates of the ocean carbon sink variability - First results of the Surface Ocean pCO_2 Mapping intercomparison (SOCOM). *Biogeosciences*, *12*(23), 7251–7278. https://doi.org/10.5194/bg-12-7251-2015

Rödenbeck, C., Keeling, R. F., Bakker, D. C. E., Metzl, N., Olsen, A., Sabine, C., & Heimann, M. (2013). Global surface-ocean pCO_2 and sea-air CO_2 flux variability from an observation-driven ocean mixed-layer scheme. *Ocean Science*, *9*(2), 193–216.Retrieved from. https://doi.org/10.5194/os-9-193-2013

Roemmich, D., & Gilson, J. (2009). The 2004–2008 mean and annual cycle of temperature, salinity, and steric height in the global ocean from the Argo program. *Progress in Oceanography*, *82*(2), 81–100. https://doi.org/10.1016/j.pocean.2009.03.004

Sarmiento, J. L., & Gruber, N. (2013). *Ocean biogeochemical dynamics*. Princeton University Press. Retrieved from https://www.jstor.org/stable/10.2307/j.ctt3fgxqx

Takahashi, T., Sutherland, S. C., Sweeney, C., Poisson, A., Metzl, N., Tilbrook, B., et al. (2002). Global sea–air CO_2 flux based on climatological surface ocean pCO_2, and seasonal biological and temperature effects. *Deep Sea Research Part II: Topical Studies in Oceanography*, *49*(9–10), 1601–1622. https://doi.org/10.1016/S0967-0645(02)00003-6

Takahashi, T., Sutherland, S. C., Wanninkhof, R., Sweeney, C., Feely, R. A., Chipman, D. W., et al. (2009). Climatological mean and decadal change in surface ocean pCO_2, and net sea-air CO_2 flux over the global oceans. *Deep Sea Research Part II: Topical Studies in Oceanography*, *56*(8–10), 554–577. https://doi.org/10.1016/j.dsr2.2008.12.009

Tomczak, M., & Liefrink, S. (2005). Interannual variations of water mass volumes in the Southern Ocean. *Journal of Atmospheric & Ocean Science*, *10*(1), 31–42. https://doi.org/10.1080/17417530500062838

van Heuven, S., Pierrot, D., Rae, J., Lewis, E., & Wallace, D. (2011). *MATLAB program developed for CO_2 system calculations. ORNL/CDIAC-105b*. Carbon Dioxide Information Analysis Center, Oak Ridge National Laboratory, U.S. Department of Energy. https://doi.org/10.3334/CDIAC/otg.CO2SYS_MATLAB_v1.1

Weiss, R. F. (1974). Carbon dioxide in water and seawater: The solubility of a non-ideal gas. *Marine Chemistry*, *2*(3), 203–215. https://doi.org/10.1016/0304-4203(74)90015-2